COUPLED MECHANICAL AND FLUID FLOW ANALYSIS IN FRACTURED SATURATED POROUS MEDIA USING THE EXTENDED FINITE ELEMENT METHOD

MARIELA LUEGE[†], JAVIER LUCERO[†] , CELESTE TORRIJOS[⋆] ,
AND ANTONIO ORLANDO[†].

Abstract. In this paper, we study the mathematical model of the steady state fluid flow in a porous media with a single crack. Two models are considered and compared: a semianalytical one which solves the general potential solution of the singular integral equation modelling the steady-state flow in a cracked porous medium, and a numerical one based on the Extended Finite Element Method (X-FEM). The semi-analytical model is used to verify the application of the X-FEM. We include then the coupling with the mechanical response of the specimen, which is analyzed using only the X-FEM. Several numerical experiments are then carried out which illustrate the variation of the hydro-mechanical quantities around the crack and within the crack.

Keywords: Fractured porous media; steady-state fluid flow; Biot-Coussy model, singular integral equation; eXtended Finite Element Method.

1. Introduction

The analysis of the hydro-mechanical behaviour of saturated fractured porous media is significant in many engineering applications, such as flow transport in geologic media, hydraulic fracturing for petroleum engineering and mining industry, permeability analysis for damage estimation, enviromental engineering, just to mention few. Given its relevance to the applications, this problem has received much attention in the scientific comunity and has been analysed from the experimental, analytical and numerical point of view.

The experimental studies carried out on the steady-state flow in fractured rocks, geological formations or concrete under given farfield conditions, provide information on the effective permeability of the medium, the connected voids and the interconnection with macro and micro cracks of the material under study. Experiments on water permeability and its variation with crack opening on saturated concrete especimens are reported in [1], where the splitting tensile test (Brazilian test) has been used for concrete fracturing tests. Further experimental results on permeability of damaged concrete can be found in [16], where the concrete specimens deteriorate as a result of the exposition to cycles of high and low temperature conditions, and of alkali-silice reactions. The final aim of these experiments is to quantify the level of deterioration of a material from its transport properties. Since the ocurrence of damage modifies the elastic properties and permeability of the material, the importance of studying cracking processes and its influence on the fluid flow is of major interest for the durability analysis of structures.

Exact analytical solutions have been obtained mainly for steady state conditions. Under these assumptions, the poroelasticty equations decouple into the Laplacian equation for the pressure, and the linear elastic equations for the effective stresses. Both elliptic equations are posed over a domain of no-Lipschitz type, with cracks lines, hence

Corresponding author: Mariela Luege, mluege@herrera.unt.edu.ar.

the classical methods for potential equations on singular domains, such as the complex variable methods and the integral transform methods, apply. Notably applications are the one by [15] that determine the stress field of an edge dislocation in a poroelastic solid by applying the Gousat potential function, by applying similar methods to those used in linear fracture analysis, and the one by [9] that apply the theory of complex potentials and the theory of Cauchy integrals In this latter work, the authors consider a domain with no-intersecting cracks and assume different boundary conditions on the cracks, in the form of either a given fluid pressure or a given pressure gradient on the crack opposite faces. In [9] the general governing equations are reduced to a singular integral equation which are solved by applying the Gauss-Chebyshev integration method. In [13, 14] this method is then extended to intersecting cracks with discharge along the cracks and to anisotropic porous body.
The numerical methods as the finite element method has been used to solve this problem as for example in [5, 6, 11] where the model to describe fractures in a saturated porous solid is proposed through the concept of partition of unity. The space of shape functions is augmented by specialized enrichment functions that are able to reproduce the discontinuous and singular elastic fields associated with the crack. These enrichment functions are introduced only to the elements in the vicinity of the fracture and its tips. This method has been originally proposed by Belytshko and Black [3] and Moes et al.[10] and is well known as XFEM. Other numerical approaches can be found in Clari and Armero [2] such as the boundary element method.
Our interest is not only in studying the fluid flow in a fractured saturated porous media but in assessing the state of stresses obtained by the numerical method. A generally accepted physical model for this problem consists in idealizing the porous saturated media as a mixture of the two phases, the fluid and the solid, which exist simultanously at each point in space but they do not mix each other. Only the fluid is allowed to leave the domain, considered then as open space. Since the fractures are very permeable layers where the pressure applied by the fluid within the cracks is equilibrated with pressure of the fluid within the pores, this allows the pore pressure to be continuous at matrix fracture interface. Nevertheless, the presence of a crack introduces two new boundaries, the opposite faces of the crack, and a new domain bounded by the faces. We will later assume that this new domain is filled up only with the fluid, no solid phase is considered. If the crack intersects the external boundary of the body, boundary conditions related to the flow need then to be added. The amount of fluid that flows from the porous faces to the crack can be determined and related to the jump in the pressure gradient. This fact can be simulated by enlarging also the space of the pressure field in such a way that the gradient of the pressure is discontinuous in the crack. The advantage of using XFEM is that this method facilitates the modelling of propagating cracks.
Hence, for the numerical resolution of this type of problem, several aspects need to be taken into account, as follows: (i) the mechanical deformation of a material under mechanical loading, in particular the action of fluid (ii) for porous material, the flow of fluid inside the porous space. (iii) assuming the presence of cracks within the material, mechanical deformation of the crack faces due to the pressure induced by the fluid, (iv) the fluid flow inside the crack.
To gain insight into the numerical tools available to simulate this type of problems, three numerical examples are solved and analysed with the proposed solution methods. For one of the examples, the comparison with available experimental observations on the subject is also presented. Hence, the paper is written as follows: first, the fluid flow problem through out a fractured porous media is formulated as an initial boundary

value problem in Section 2, afterwards the problem is solved following two fronts, a numerical one and a semianalytical, Sections 3 and 4, respectively. Finally, in Section 5.4, two numerical examples aim to compare both methods, a third example couples fluid and mechanical response, whereas the last example compares the X-FEM with experimental meassurements.

2. Governing equations of fractured porous media

In this section we present the strong form of the equations governing the diffusion of fluid through a deformable fractured porous media. The basic assumptions in the derivation are: small deformations, negligible convective and inertial terms, homogeneous and isotropic solid matrix and saturated conditions. We will focus on the classical formultion of fluid flow in porous media as proposed by Coussy [7], including discontinuities or cracks in the solid matrix by introducing new boundary conditions on the flow and pressure due to the presence of the crack.

The saturated porous media is considered as the superimposition of two continua or phases, a porous solid and a fluid, at each infinitesimal volume. To determine the flow and pressure distribution of the fluid and the deformation of the solid phase all over the space, we need to introduce the mass balance equation and the balance of linear momentum for each phase, together with the constitutive equations and boundary conditions.

Let $\Omega \in \mathbb{R}^2$ be a reference volume of a saturated porous media made of a solid and a fluid phase. Denote then by $\rho_s(\boldsymbol{x}, t)$ and $\rho_f(\boldsymbol{x}, t)$ the solid and fluid mass density, respectively, and by $n \in [0, 1]$ the solid porosity whereas $n\mathrm{d}\Omega$ represents the volume ocuppied by the fluid in a differential volume of the saturated porous media domain Ω, assuming no mass exchange between the solid and the fluid. Let also consider the presence of a crack Γ in Ω. This crack can end inside Ω, or on the boundary $\partial\Omega$. The intersection of Γ with $\partial\Omega$ is denoted as γ. The line Γ is represented by a smooth function $\boldsymbol{z}(x^*)$, with x^* the curvilinear parameter. No intersection of cracks will be considered in this work. Since $\Gamma \subset \Omega$, the set of points $\boldsymbol{x} \in \Omega \setminus \Gamma$ are called matrix points, whereas $\boldsymbol{z} \in \Gamma$ are points located at the cracked surface. The orientation of such surface is defined by the normal $\boldsymbol{n}_\Gamma$ to the tangent plane at $\boldsymbol{z} \in \Gamma$ (see Figure 1).

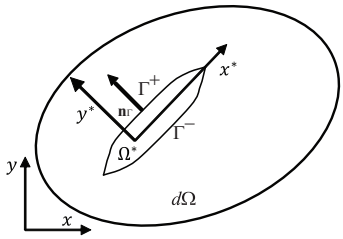

Figure 1. Infinitesimal volume of a porous medium, superimposing a porous solid phase with porous space filled with fluid.

The mass balance of the solid phase integrated in Ω, with $\partial\Omega$ its boundary, using the Reynolds transport theorem can be expressed in the form

$$\frac{d^s}{dt}\int_\Omega (1-n)\rho_s \mathrm{d}\Omega = \int_\Omega (1-n)\frac{\partial \rho_s}{\partial t} + \int_{\partial\Omega} (1-n)\rho_s \boldsymbol{v}_s \cdot \boldsymbol{n}\mathrm{d}\Omega = 0\,, \tag{2.1}$$

where $\boldsymbol{v}_s$ is the solid velocity and $\boldsymbol{n}$ the unit normal to the boundary $\partial\Omega$. We note that for an incompressible solid matrix, $\partial\rho_s/\partial t = 0$ with $n = n(\boldsymbol{x})$, therefore we can deduce that $\nabla \cdot \boldsymbol{v}_s = 0$ in uncracked solid phase.

Analogously for the fluid phase, the integral form of the mass balance in Ω reads

$$\frac{d^f}{dt}\int_\Omega n\rho_f \mathrm{d}\Omega = \int_\Omega \frac{\partial(n\rho_f)}{\partial t}\mathrm{d}\Omega + \int_{\partial\Omega}(n\rho_f)\boldsymbol{v}_f\cdot\boldsymbol{n}\mathrm{d}\Omega + \int_\gamma \rho_f \boldsymbol{q}\cdot\boldsymbol{m}\mathrm{d}l = 0 \tag{2.2}$$

with $\boldsymbol{v}_f$ the fluid velocity $n\boldsymbol{v}_f\cdot\boldsymbol{n}$ is the flux passing through $\partial\Omega$ and $\boldsymbol{m} = \partial\boldsymbol{z}/\partial x^*$ the unit vector tangent to the crack surface or line. We can therefore denote as $q = \boldsymbol{q}\cdot\boldsymbol{m} = \int_{-h}^{h} v(y^*)\mathrm{d}y^*$ the flux leaving the crack on γ, which is calculated as the integral of the tangential component of fluid velocity $v = \boldsymbol{v}_f\cdot\boldsymbol{m}$, in the thickness of the crack. Since we have included a discontinuity in Ω, the divergence theorem for the vector field $\boldsymbol{v}_f$ in Ω and $\boldsymbol{q}$ in Γ take the form

$$\begin{aligned}
&\textstyle\int_{\partial\Omega}(n\rho_f)\boldsymbol{v}_f\cdot\boldsymbol{n}\mathrm{d}s = \int_{\Omega\setminus\Gamma}\nabla\cdot(n\rho_f\boldsymbol{v}_f)\mathrm{d}\Omega - \int_\Gamma (n\rho_f)[\![\boldsymbol{v}_f]\!]\cdot\boldsymbol{n}_\Gamma\mathrm{d}\Omega\\
&\textstyle\int_\gamma \rho_f\boldsymbol{q}\cdot\boldsymbol{m}\mathrm{d}l = \int_\Gamma \nabla_{x^*}\cdot(\rho_f\boldsymbol{q})\mathrm{d}\Gamma
\end{aligned} \tag{2.3}$$

with $\boldsymbol{n}_\Gamma$ the unit normal to the discontinuity Γ pointing to Γ^+. The notation $[\![*]\!] = *^+ - *^-$ represents the difference between of values of $*$ at opposite faces of the crack, Γ^+ and Γ^- respectively, therefore part of the flow in the porous media that passes Γ^- joins the flow inside the crack, $\nabla_{x^*}\cdot\rho_f\boldsymbol{q}$ is the surface divergence of $\rho_f\boldsymbol{q}$. The first integral, at the right hand side of the equality sign in (2.2), is written as the sum of the following integrals in $\Omega\setminus\Gamma$ and Γ

$$\int_\Omega \frac{\partial(n\rho_f)}{\partial t}\mathrm{d}\Omega = \int_{\Omega\setminus\Gamma}\frac{\partial(n\rho_f)}{\partial t}\mathrm{d}\Omega + \int_\Gamma \frac{\partial(2h\rho_f)}{\partial t}\mathrm{d}\Gamma \tag{2.4}$$

where $n = 1$ inside the integral over Γ, h is half the crack thickness and $2h\rho_f$ represents the fluid mass content per unit surface of the crack. Replacing (2.3) and (2.4) into (2.2) we obtain the following

$$\int_{\Omega\setminus\Gamma}\left[\frac{\partial(n\rho_f)}{\partial t} + \nabla\cdot(n\rho_f\boldsymbol{v}_f)\right]\mathrm{d}\Omega + \int_\Gamma\left[n\rho_f[\![\boldsymbol{v}_f]\!]\cdot\boldsymbol{n}_\Gamma + \frac{\partial(2h\rho_f)}{\partial t} + \nabla_{x^*}\cdot(\rho_f\boldsymbol{q})\right]\mathrm{d}\Gamma = 0 \tag{2.5}$$

The mass balance in local form is written as follows

$$\begin{aligned}
&\frac{\partial(n\rho_f)}{\partial t} + n\rho_f\nabla\cdot\boldsymbol{v}_s + \nabla\cdot n\rho_f(\boldsymbol{v}_f - \boldsymbol{v}_s) = 0 \quad \forall\boldsymbol{x}\in\Omega\setminus\Gamma\\
&\frac{\partial(2h\rho_f)}{\partial t} + \rho_f[\![\boldsymbol{v}_f]\!]\cdot\boldsymbol{n}_\Gamma + \nabla_{x^*}\cdot(\rho_f\boldsymbol{q}) = 0 \quad \forall\boldsymbol{z}(x^*)\in\Gamma\setminus\gamma
\end{aligned} \tag{2.6}$$

Allowing the fluid to be compressible, $n\frac{\mathrm{d}\rho_f}{\rho_f} = \frac{\mathrm{d}p}{K_f}$ the mass balance equations (2.6) in a saturated porous media can be reduced to the following equation

$$\frac{1}{K_f}\frac{\partial p}{\partial t} + n\nabla\cdot\boldsymbol{v}_s + \nabla\cdot n(\boldsymbol{v}_f - \boldsymbol{v}_s) = 0 \quad \forall\boldsymbol{x}\in\Omega\setminus\Gamma \tag{2.7}$$

Having neglected the inertial terms, the momentum balance for the fluid phase reduces to the linear motion equation known as Darcy's law

$$n(\boldsymbol{v}_f - \boldsymbol{v}_s) = \frac{k}{\mu}(-\nabla p + \rho_f\boldsymbol{b}) \tag{2.8}$$

with k intrinsic isotropic permeability of the porous matrix, μ the dynamic viscosity of the fluid and $\boldsymbol{b}$ is the body force per unit mass vector.
The flow model in cracks is commonly described by the Poiseuille type of law, where the flux vector is linearly related to inplane pressure gradient inside the crack, and defined as follows

$$q(x^*) = -k_d \nabla_{x^*} p(x^*) \tag{2.9}$$

with $\nabla_{x^*} p = \partial p / \partial \boldsymbol{z} \cdot \boldsymbol{m}$ and k_d the hydraulic conductivity. For the laminar flow between two infinite and parallel planes, the conductivity is determined as $k_d = \frac{1}{f}\frac{(2h)^3}{12\mu}$, with $2h$ the crack aperture and f a coefficient that depends on the rugosity of the crack surface. We can note that $k_d \to \infty$ correspond to very high conductivity and constant pressure along the crack, simulating the case of void crack.
Finally, we introduce the momentum balance over the saturated porous media domain Ω as follows

$$\int_{\partial\Omega} \boldsymbol{\sigma} \cdot \boldsymbol{n} \mathrm{d}a + \int_{\Omega} \rho \boldsymbol{b} \, \mathrm{d}\Omega = 0 \tag{2.10}$$

where $\bar{\boldsymbol{t}} = \boldsymbol{\sigma} \cdot \boldsymbol{n}$ and $\rho = (1-n)\rho_s + n\rho_f$ is density of the mixture. The macroscopic total stress tensor $\boldsymbol{\sigma} = (1-n)\boldsymbol{\sigma}_s + np\mathbf{1}$ is also obtained using the mixture theory, which relates through averaging procedures, the microscopic stress field with the macroscopic stress, i.e. $\boldsymbol{\sigma}_s$ is the averaged stress acting in the solid matrix and np the averaged fluid pressure applied on the internal walls of solid matrix. Equation (2.10) written in local form

$$\nabla \cdot \boldsymbol{\sigma} + \rho \boldsymbol{b} = \mathbf{0} \, . \tag{2.11}$$

The constitutive equations of the porous media, composed of a deformable solid matrix and a saturating fluid, needs to be introduced. The Clausius-Duhem inequality related to deformable porous continua is of the form $\Phi = \Phi_s + \Phi_f + \Phi_{th} \geq 0$, with Φ the overall dissipation, where Φ_s, Φ_f and Φ_{th} the different sources of dissipation. The thermal dissipation Φ_{th} is not considered in this work since we have assumed isothermal conditions. Assuming that the fluid contained in $d\Omega$ changes, i.e. there is fluid mass exchange with the exterior before and after the deformation of the solid matrix, the domain is called an open system. Hence, the solid matrix dissipation Φ_s is of the form

$$\Phi_s = \boldsymbol{\sigma} : \frac{d\boldsymbol{\varepsilon}}{dt} - \phi \frac{dp}{dt} - \frac{dG_s}{dt} \tag{2.12}$$

with $G_s = G_s(\boldsymbol{\varepsilon}, p)$ the Gibbs energy and $\phi \frac{dp}{dt}$ takes into account the pore pressure acting on the matrix porous walls, ϕ is the Lagrangian porosity with $\phi d\Omega_0 = n d\Omega$, and $\phi = Jn \approx (1+\epsilon)n$ for small deformations. Assuming negligible matrix volume changes, i.e. incompresible solid matrix $\epsilon_s = 0$: $\phi = \epsilon = \mathsf{tr}\, \varepsilon$.
The disssipation related to the fluid movement with respect to the solid matrix is of the form

$$\Phi_f = -\nabla p \cdot n(\boldsymbol{v}_f - \boldsymbol{v}_s) \, . \tag{2.13}$$

Assuming that the dissipation related to elastic solid matrix Φ_s is zero the constitutive equations reduce to state equations. Linear isotropic poroelasticity is then obtained by choosing the following quadratic energy expression with respect to the first (ϵ) and second ($\boldsymbol{e} : \boldsymbol{e}$) strain invariants, with $\boldsymbol{e} = \boldsymbol{\varepsilon} - \frac{1}{3}\epsilon\mathbf{1}$

$$G_s(\epsilon, \boldsymbol{e}, p) = \frac{1}{2}K\epsilon^2 - bp\epsilon - \frac{1}{2}\frac{p^2}{N} + G\boldsymbol{e} : \boldsymbol{e} \tag{2.14}$$

Since $\boldsymbol{s} = \partial G_s/\partial \boldsymbol{e}$, $\sigma = \partial G_s/\partial \epsilon$ and $\phi = -\partial G_s/\partial p$, for a poroelastic isotropic linear solid, we obtain the constitutive equations as follows

$$\boldsymbol{\sigma} = \boldsymbol{s} + \sigma \mathbf{1} = 2G\boldsymbol{e} + (K\epsilon - bp)\mathbf{1}\,; \quad \phi = b\epsilon - \frac{p}{N} \tag{2.15}$$

G and K denote the shear and volumetric elastic modulus, respectively; $b = 1 - K/K_s \leq 1$ the Biot's coefficient and $1/N = (b - \phi_0)/K_s$ the Biot's modulus, ϕ_0 initial porosity, K denotes the bulk moduli of the porous medium and K_s of the solid grains (see [15] for more details).

To complete the formulation of the initial boundary value problem, the boundary and initial values of the field variables need to be specified. Classically the boundary $\partial\Omega$ of a continuum body is subdivided into two parts, the part where the primary variables are prescribed, in our case $\partial_u\Omega$ y $\partial_p\Omega$ and where the traction and velocities are prescribed, respectively $\partial_t\Omega$ and $\partial_v\Omega$.

It is assumed that both porous space and cracks are saturated, pressure across the crack is constant, and there is no pressure jump across the faces of fracture (continuity of the pressure field).

Given the initial conditions on the solid displacement, the fluid velocity and pressure, the problem is formulated as follows:

Find $\boldsymbol{u}$, $\boldsymbol{v}_f$ and p in $\Omega \setminus \Gamma$, bounded by $\partial\Omega$ and Γ, and the flux $\boldsymbol{q}$ inside Γ, such that the following equations re satisfied

Balance equations:

$$\frac{1}{K_f}\frac{\partial p}{\partial t} + n\nabla \cdot \boldsymbol{v}_s + \nabla \cdot n(\boldsymbol{v}_f - \boldsymbol{v}_s) = 0 \qquad \forall \boldsymbol{x} \in \Omega \setminus \Gamma \quad \text{eq. } (2.6)_1$$

$$\frac{\partial(2h\rho_f)}{\partial t} + \rho_f[\![\boldsymbol{v}_f]\!] \cdot \boldsymbol{n}_\Gamma + \nabla_{x^*} \cdot (\rho_f \boldsymbol{q}) = 0 \quad \forall \boldsymbol{z} \in \Gamma \setminus \gamma \quad \text{eq. } (2.6)_2$$

$$\nabla \cdot \boldsymbol{\sigma} + \rho \boldsymbol{b} = \mathbf{0} \qquad \forall \boldsymbol{x} \in \Omega \qquad \text{eq. } (2.11)$$

$$n(\boldsymbol{v}_f - \boldsymbol{v}_s) = \frac{k}{\mu}(-\nabla p + \rho_f \boldsymbol{b}) \qquad \forall \boldsymbol{x} \in \Omega \setminus \Gamma \quad \text{eq. } (2.8)_1$$

$$q = -k_d \nabla_{x^*} p \qquad \forall \boldsymbol{z} \in \Gamma \qquad \text{eq. } (2.9)$$

Constitutive laws:

$$\boldsymbol{\sigma} = 2G\boldsymbol{e} + (K\epsilon - bp)\mathbf{1} \qquad \forall \boldsymbol{x} \in \Omega \qquad \text{eq. } (2.15)_1$$

$$\phi = b\epsilon - \frac{p}{N} \qquad \forall \boldsymbol{x} \in \Omega \qquad \text{eq. } (2.15)_2$$

Boundary conditions:

$$p = \bar{p} \qquad \forall \boldsymbol{x} \in \partial_p\Omega$$

$$\boldsymbol{u} = \bar{\boldsymbol{u}} \qquad \forall \boldsymbol{x} \in \partial_u\Omega$$

$$n(\boldsymbol{v}_f - \boldsymbol{v}_s) \cdot \boldsymbol{n} = \bar{v} \qquad \forall \boldsymbol{x} \in \partial_v\Omega$$

$$\boldsymbol{\sigma} \cdot \boldsymbol{n} = \bar{\boldsymbol{t}} \qquad \forall \boldsymbol{x} \in \partial_t\Omega$$

$$\boldsymbol{\sigma} \cdot \boldsymbol{n}_\Gamma = -\bar{p}\boldsymbol{n}_\Gamma \qquad \forall \boldsymbol{z} \in \Gamma$$

$$\boldsymbol{q} \cdot \boldsymbol{m} = \bar{q} \qquad \forall \boldsymbol{z} \in \gamma$$

with $\boldsymbol{u}$ the displacement vector of the solid, $\boldsymbol{v}_s = d\boldsymbol{u}/dt$ the solid velocity vector and $\bar{v}$ is the normal relative velocity prescribed on $\partial_v\Omega$. The points in γ where the crack intersects the boundary prescribes the discharge $\bar{q}$. Also, the usual conditions on the boundaries are verified: $\partial_v\Omega \cup \partial_p\Omega = \partial\Omega$ and $\partial_t\Omega \cup \partial_u\Omega = \partial\Omega$. The extreme points of a crack constitute a set a singular points.

For the solution of the problem two solution methods will be used and compared, a semianalytical approach and a numerical approach. In the former one, cracks are assimilated to a repartition of point sources. Therefore the analytical solution is known in terms of a singular integral equation, which is solved numerically. For the numerical approach, the so called eXtended Finite Element Method (XFEM) is employed. In this case the displacement and pressure field variables are enriched locally by introducing the near tip asymptotic solutions, displacement and pressure gradient discontinuity jumps, through out the partition of unity property of the shape functions.

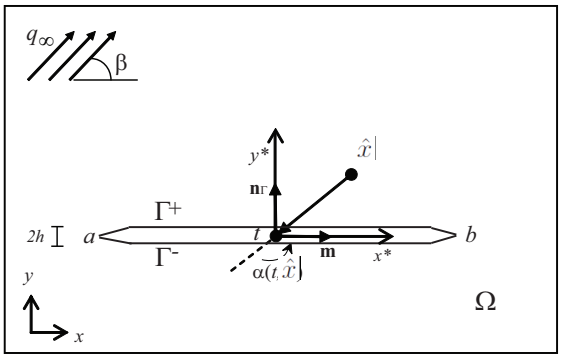

FIGURE 2. Single crack in an infinite plate. Distance from each point in the crack to a point $z = x + iy$ on the plane.

3. Semianalitical solution of the flow problem in porous cracked problem

3.1. **General analytical solution of the problem.** The analytical resolution of a 2D fluid flow in fractured porous medium, as deduced by [9] and [13], is presented in this section for different boundary conditions along the crack. Assuming an isotropic saturated porous domain Ω that is infinite, and contains a discontinuity Γ as shown

in Figure 2, for a flow under steady-state regime, the mass balance (2.6) is reduced to the Laplace equation

$$\Delta p = \frac{\partial^2 p}{\partial x^2} + \frac{\partial^2 p}{\partial y^2} = 0 \quad \forall (x, y) \in \Omega \setminus \Gamma. \tag{3.1}$$

The general solution of (3.1), see [12] for plane strain elasticity equations expressed in terms of Goursat Muskhelishvili potential functions of the complex variable, is given as

$$\begin{aligned} p(x, y) &= 2\mathrm{Re}(\Phi(x, y)) \\ \text{with } \Phi(\hat{x}) &= \frac{q_\infty}{2} \hat{x}\, e^{-i\beta} + \bar{\Phi}(\hat{x}) \end{aligned} \tag{3.2}$$

with Φ the pressure potential of the steady state fluid flow, an analytic complex function in terms of $\hat{x} = x + iy$, $i = \sqrt{-1}$, q_∞ homogeneous fluid flow, β angle between the flow and the x-axis. The boundary conditions along the crack's opposite faces can then be introduced, either as known pressure or fluid velocity.
Let consider first the case where the pore pressure $\bar{p}$ along the crack is given, and the potential function has the form

$$\bar{\Phi} = \frac{1}{2\pi} \int_\Gamma \frac{\phi(t)}{t - \hat{x}} dt \tag{3.3}$$

with $\phi(t)$ the unknown density function integrable and continuous on Γ, $t \in \Gamma$ a complex coordinate point. The potential $\bar{\Phi}$ is an integral of Cauchy type along the boundary of the crack Γ and an holomorphic function in $\Omega \setminus \Gamma$ that approaches zero for large distances $r = |t - \hat{x}|$, with ($t - \hat{x} = re^{i\theta}$ and $\theta = \arg(t - \hat{x})$).
We can then reformulate the problem as follows
Find $\phi = \phi(t)$, with $t \in \Gamma$, such that

$$\begin{aligned} p(\hat{x}) &= \frac{q_\infty}{2} \hat{x} \cos(\beta) + \frac{1}{\pi} \int_\Gamma \frac{\phi(t)}{|t - \hat{x}|} dr \quad \hat{x} \in \Gamma \\ \text{with} \qquad & p^{\pm}(t_0) = \bar{p}(t_0) \qquad t_0 \in \Gamma\,. \end{aligned} \tag{3.4}$$

the pressure induced by point sources sinks in Γ is $\bar{p}$, wheres $\pm$ denotes the limiting values of a function as the boundary approaches to $+$ or $-$ side of the crack.
Once $\phi(t)$ has been determined the pressure distribution over the domain can be easily calculated.
Let consider now a second case where the flow inside the crack is assumed of Poiseuille type, in [14], the following potential function is proposed

$$\begin{aligned} \Phi &= \frac{q_\infty}{2} \hat{x} \exp i\beta + \int_\Gamma \phi(t) \ln(\hat{x} - t) dt \\ \text{with} \quad & \phi(t(x^*)) = \frac{1}{2\pi k} \nabla_{x^*} q(t(x^*)) \end{aligned} \tag{3.5}$$

where $(3.5)_2$ is deduced from the mass balance inside the crack (equation $(2.6)_2$) and the assumption of steady state regime (see Pouya for more details). Hence, the problem is reformulated as follows

Find $q(t(x^*))$, with t, $t_0 \in \Gamma$, such that

$$p(t_0) = \frac{q_\infty}{2} t_0 \cos(\beta) + \frac{1}{2\pi k} \int_\Gamma \nabla_{x^*} q(t) \ln|t_0 - t| dt \tag{3.6}$$
$$\text{with} \quad p^{\pm}(t_0) = \int_0^{t_0} q(t)\, dt\,, \quad q(t_0) = -k_d \nabla_t p(t_0) \quad t_0 \in \Gamma\,.$$

To solve (3.4) and (3.6) approximately, direct methods can be used such as the one proposed in [8], the apropiate quadrature formula to be chosen depends on the type of singularity at the ending points a and b. At the points of geometrical singularity a and b the function ϕ can be either bounded or has an integrable singularity, and this depends on the physical arguments of the problem. When the unknown function is the pore pressure potential, as is usually the case, ϕ is bounded at the extremities. For this case in [8], the Gauss-Chebyshev quadrature formula is proposed where the points of integration $t_j \in \Gamma$ along Γ, with $i = 1, ..., N$ are the zeros of the Chebyshev polynomial of the first kind of degree N and the collocation points $\hat{x}_i \in \Omega$, with $i = 1, ..., N+1$ where pore pressure p is determined, are the zeros of the Chebyshev polynomial of second kind of degree $N + 1$.
Denoting as $w(x^*)$ the fundamental function of the singular integral equation (3.6), and $g(x^*)$ a bounded function, continuous in $s \in [a, b]$, we can write $\phi(x^*)$ as follows

$$\phi(x^*) = w(x^*) g(x^*)\,, \quad (a < x^* < b) \tag{3.7}$$

with $w(x^*) = \sqrt{(x^* - a)(x^* - b)}$. Numerical methods for the determination of $g(x^*)$ will be developed in the following subsection for different Dirichlet and Neumann boundary conditions. The value of the function ϕ is then determined at some specific nodes, which are solution of the resulting system of linear algebraic equations.

3.1.1. *Prescribed pressure inside single crack.* Let us consider a problem with Dirichlet boundary conditions, i.e. the pressure distribution inside the crack $\bar{p}(t_0)$ is known for every $t_0 \in \Gamma$, and $q_\infty = 0$ as shown in Figure 3, hence from (3.4) the following relation holds

$$\bar{p}(t_0) = \frac{1}{\pi} \int_\Gamma \frac{\phi(t)}{|t - t_0|} dr\,. \tag{3.9}$$

with $r = |t - t_0|$ and for $t = t_0$ the integral of equation is singular.
To calculate pore pressure p in $\hat{x} \in \Omega$, the unknown densities ϕ need to be defined in such a way that the boundary condition, eq. (3.9), along the crack is satisfied. Following [8, 9] for the numerical resolution, a set of collocation points $\hat{x}_i \in \Omega$, with $i = 1, ..., N + 1$, are chosen together with a set of integration points $t_j \in \Gamma$, with $j = 1, ..., N$. This method produces a discrete approximation, hence a system of $N + 1$ linear algebraic equations in N unknowns $g_j = g(t_j)$ needs then to be solved, note that equation $N/2 + 1$ can then be ignored. Denoting as t_{0i} the collocations points $\hat{x}_i \in \Gamma$, i.e. $t_{0i} = \hat{x}_i$.

$$\bar{p}(t_{0i}) = \frac{1}{\pi} \sum_{j=1}^{N} w_j \frac{g_j}{|t_j - t_{0i}|}\,, \quad i = 1, ..., N + 1 \tag{3.10}$$

$$w_j = w(t_j) = \frac{\pi}{N+1} \sin^2\left(\frac{j\pi}{N+1}\right) \tag{3.11}$$

The fundamental function w_j is selected in such a way to result the corresponding weight function and t_j are then called the integration points and correspond to the

(3.8)

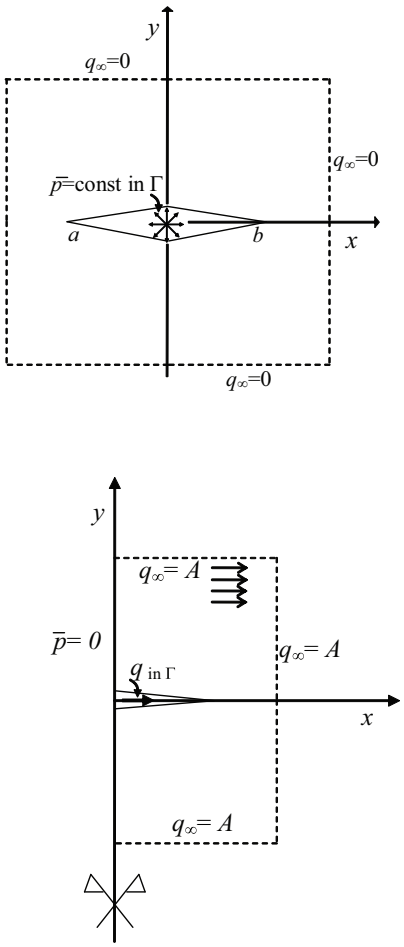

FIGURE 3. Single crack in an infinite plate: (a) Subjected to constant pressure, (b) Subjected to .

zeros of the orthogonal polynomials related to the particular Gaussian quadrature. For the case of integrable singularities at the end points, the orthogonal polynomials reduce to the Chebyshev polynomials of first kind are written

$$t_j = \frac{b-a}{2}\zeta_j + \frac{b+a}{2} \qquad t_{0i} = \frac{b-a}{2}\eta_i + \frac{b+a}{2} \tag{3.12}$$

ζ_j the integration points, roots of the Chebyshev polynomials of second kind and order N, η_i collocation points, roots of the Chebyshev polynomials of the first kind and order $(N+1)$ refering to an interval $[-1,1]$ as follows with and

$$\zeta_j = \cos\left(\frac{j\pi}{N+1}\right),\ j=1,...,N \quad ; \quad \eta_i = \cos\left(\frac{\pi(2i-1)}{2(N+1)}\right),\ i=1,...,N+1 \tag{3.13}$$

Once g_j is determined, the pressure and the gradient of the pressure in the entire domain Ω is calculated as follows

$$
\begin{aligned}
p(\hat{x}_i) &= \frac{1}{\pi}\sum_{j=1}^{n} w_j \frac{g_j}{|t_j - \hat{x}_i|} \\
\nabla_{\hat{x}} p(\hat{x}_i) &= \frac{1}{2}\left(\frac{\partial p(\hat{x}_i)}{\partial x} - i\frac{\partial p(\hat{x}_i)}{\partial y}\right) \\
&= \frac{1}{2\pi}\sum_{j=1}^{n} w_j g_j \frac{\cos\alpha(t_j,\hat{x}_i)}{|t_j - \hat{x}_i|^2} - i\frac{1}{2\pi}\sum_{j=1}^{n} w_j g_j \frac{\sin\alpha(t_j,\hat{x}_i)}{|t_j - \hat{x}_i|^2}
\end{aligned} \tag{3.14}
$$

α is the angle formed by the vector $t_j\hat{x}$ and the axis $O\hat{x}$. The complete algorithm is summarized in Box 1.

Box 1. Numerical Integration Algorithm for Semianalytical Resolution

Given: $a,\ b,\ N,\ M$ and $p(t_{0i}) = \bar{p} \quad \forall t_{0i} \in \Gamma\,, \quad i = 1, ..., N+1;$

with $t_{0i} = \dfrac{b-a}{2}\eta_i + \dfrac{b+a}{2}$ and $\eta_i = \cos\left(\dfrac{\pi(2i-1)}{2(N+1)}\right)$

Compute: for $j = 1, ..., N$

$$w_j = \frac{\pi}{n+1}\sin^2\left(\frac{j\pi}{N+1}\right)$$

$$t_j = \frac{b-a}{2}\zeta_j + \frac{b+a}{2}$$

$$\zeta_j = \cos\left(\frac{j\pi}{N+1}\right)$$

$$B_{ij} = \frac{w_j}{|t_j - t_{0i}|}\,,$$

Solve: $g(t_j) = [B_{ij}]^{-1} p(t_{0i})$

Find: $\forall \hat{x}_k \in \Omega \setminus \Gamma, \quad$ with $\quad k = 1, ..., M$

$$p(\hat{x}_k) = \frac{1}{\pi}\frac{w_j g_j}{|t_j - \hat{x}_k|}$$

$$\nabla_{\hat{x}} p(\hat{x}_k) = \frac{1}{2\pi}\sum_{j=1}^{N} w_j g_j \frac{\cos\alpha(t_j,\hat{x}_k)}{|t_j - \hat{x}_k|^2} - i\frac{1}{2\pi}\sum_{j=1}^{N} w_j g_j \frac{\sin\alpha(t_j,\hat{x}_k)}{|t_j - \hat{x}_k|^2}$$

End

3.1.2. *Poiseuille flow inside the crack.* Let here consider again the problem of a single straight crack Γ in a porous domain but under constant pressure gradient at an infinite boundary and a flux q inside Γ is of Poiseuille type.
Assuming then that the fluid flow at the infinite boundary is of the form $q_\infty(x, y) = A$, and placing the origin of the coordinate system at the center of the crack (see Figure 2.9), $x^* \equiv x$, the symmetry on the geometry and the boundary lead to $p(-x, y) = -p(x, y)$, $q(-x) = -q(x)$ and $p(0, 0) = 0$. Therefore the pressure at a point Γ with complex coordintes $t_0 = x_0 + 0i$ can be calculated as the integral of the pressure gradient along the crack, as follows

$$p(x_0, 0) = \int_0^{x_0} \nabla_x p\, dx \tag{3.15}$$

We have assumed pressure pore continuity from the porous matrix to the crack cavity through $\boldsymbol{\sigma} \cdot \boldsymbol{n}_\Gamma = -\bar{p}\boldsymbol{n}_\Gamma$ and fluid flow through the discontinuity faces. The part of the fluid coming from the porous matrix through the crack faces flow away in the cavity, introduces a discontinuity jump in the normal fluid flow.
Since the integral term of (3.15) is the only that contributes to the discontinuity jump of the pressure gradient across the crack, as deduced in [13], the following relation satisfies the balance equations for a point on the crack Γ at the absice x,

$$\phi(x) = \frac{1}{2\pi k}\nabla_x q(x) \tag{3.16}$$

Replacing (3.16) in equation (3.15) and integrating by parts the integral over Γ takes the form

$$\frac{1}{2\pi k}\int_a^b \nabla_x q(x) \ln|x_0 - x| dx = \frac{1}{2\pi k}\left[q(x)\ln|x_0 - x|\right]_a^b - \frac{1}{2\pi k}\int_a^b q(x)\nabla_x \ln|x_0 - x| dx \tag{3.17}$$

The contribution of the first term on the r.h.s of (3.17), together with the Poiseuille law $q = -k_d \nabla_x p$, the solution takes the form

$$p(x_0) = Ax_0 + \frac{k_d}{2\pi k}\int_a^b \nabla_x p \frac{x_0 - x}{|x_0 - x|^2} dx \tag{3.18}$$

By taking $a = -1$ and $b = 1$, the unknown function $\nabla_x p$ will be obtained numerically by first rewritting $\nabla_x p(x) = w(x)g(x)$, where $g(x)$ is a bounded continuous function in $[-1, 1]$. Due to the singular character of equation (3.19), the problem is formulated at x_0 using (3.15) and (3.19) as follows $\forall x_0 \in [0, 1]$

$$\begin{aligned}
p(x_0) - \frac{k_d}{2\pi k}\int_{-1}^{1} \frac{\nabla_x p(x)}{x_0 - x} dx &= Ax_0 \\
\int_0^{x_0} \nabla_x p dx - \frac{k_d}{2\pi k}\int_{-1}^{1} \frac{\nabla_x p(x) - \nabla_x p(x_0)}{x_0 - x} dx - \frac{k_d}{2\pi k}\nabla_x p(x_0)\ln\frac{1 - x_0}{1 + x_0} &= Ax_0 \\
\int_0^{x_0} \nabla_x p dx + \frac{k_d}{\pi k}\int_0^1 (\nabla_x p(x) - \nabla_x p(x_0))\frac{x_0}{x^2 - x_0^2} dx - \frac{k_d}{2\pi k}\nabla_x p(x_0)\ln\frac{1 - x_0}{1 + x_0} &= Ax_0
\end{aligned} \tag{3.19}$$

and the problem is formulated as follows
Find $g(x_0)$, $\forall x_0 \in [0, 1]$, such that

$$\int_0^{x_0} w(x)g(x)dx - \frac{k_d x_0}{\pi k}\int_0^1 w(x)\frac{g(x) - g(x_0)}{x^2 - x_0^2} dx - \frac{k_d}{\pi k}g(x_0)\ln\frac{1 - x_0}{1 + x_0} = Ax_0 \tag{3.20}$$

where the singularity at the extremity has been removed. For the solution of the problem we will use a quadrature formula of Gaussian type. Evaluating the integral at x_{0i} $(i = 1, ..., N+1)$, so called collocation points, we reduce the problem to a system of linear equations in $g_j = g(x_j)$, $j = 1, ..., N$ unknowns, with x_j the integration points.

$$\sum_{j=1}^{i} w_j g_j - \frac{x_{0i}k_d}{\pi}\sum_{k=1}^{N} w_k \frac{g_k - g_{0i}}{x_k^2 - x_{0i}^2} - \frac{k_d}{2\pi} g_{0i}\ln\frac{1 - x_{0i}}{1 + x_{0i}} = k\, x_{0i} \tag{3.21}$$

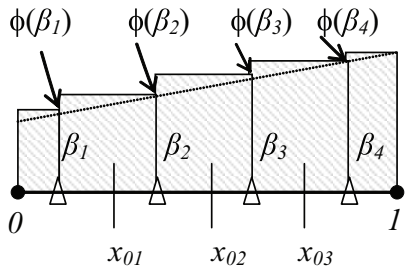

FIGURE 4. Integration and collocation points along the crack for $N = 3$.

with $i = 1, ..., N+1$, , $w_i = x_{0i} - x_{0(i-1)}$ the last equation can be rewritten as a system of discrete linear system,

$$\sum_{j=1}^{N} B_{ij} g_j - A x_{0i} = 0 \quad \forall i = 1, ..., N+1 \tag{3.22}$$

$$\begin{aligned} B_{ij} &= w_j - \frac{k_d}{\pi} T_{ij} && \text{if } j < i \\ B_{ii} &= \frac{1}{2} w_j - \frac{k_d}{\pi} \sum_{k=1}^{N} T_{ik} - \frac{k_d}{2\pi} g_{0i} \log \frac{1 - x_{0i}}{1 + x_{0i}} && \text{if } i = j \\ B_{ij} &= -\frac{k_d}{\pi} T_{ij} && \text{if } j > i \end{aligned}$$

with $T_{ij} = \dfrac{w_j x_{0i}}{x_j^2 - x_{0i}^2}$, if $i \neq j$; $T_{ii} = 0$, if $i = j$.

Once (3.21) has been solved, the pressure at any point $\hat{x} \in \Omega$ can be calculated by integrating numerically the equation

$$p(\hat{x}) = A x + \frac{k_d}{2\pi k} \int_0^1 w(x) g(x) \left[\frac{t(x) - \hat{x}}{|t(x) - \hat{x}|^2} - \frac{t(x) + \hat{x}}{|t(x) + \hat{x}|^2} \right] dx \,, \tag{3.23}$$

as follows

$$p(\hat{x}_i) = A x_i + \frac{k_d}{2\pi k} \sum_{j=1}^{N} w_j g_j \left[\frac{t_j - \hat{x}_i}{|t_j - \hat{x}_i|^2} - \frac{t_j + \hat{x}_i}{|t_j + \hat{x}_i|^2} \right] . \tag{3.24}$$

4. Numerical solution of the hydromechanical coupled problem

The solution of the problem using the X-FEM will be presented in this section. This method has been developed with the aim of taking into account discontinuities, and its propagation, in the displacement field due to fractures, by enlarging the space of the displacement field through the introduction of enrichment functions. This method has been extended to the case of fluid transport by enriching also the pressure field.

4.1. **Weak form of the governing equations.** In light of the momentum and fluid mass balance eqution (2), the mixed variational formulation at a time instant $t = t_{n+1}$ takes the form

Box 2. Numerical Integration Algorithm for Semianalytical Resolution

GIVEN: a, b, N, M and $q_\infty = A$

Compute: for $j = 1, ..., N$; $i = 1, ..., N+1$

$$x_{0i} = \frac{b-a}{2}\eta_i + \frac{b+a}{2}; \quad \eta_i = \cos\left(\frac{\pi(2i-1)}{2(N+1)}\right)$$

$$w_i = x_{0i} - x_{0(i-1)}$$

$$x_j = \frac{b-a}{2}\zeta_j + \frac{b+a}{2}; \quad \zeta_j = \cos\left(\frac{j\pi}{N+1}\right)$$

$$\text{if } i \neq j, \quad T_{ij} = \frac{w_j x_{0i}}{x_j^2 - x_{0i}^2},$$

$$\text{if } i = j, \quad T_{ii} = 0,$$

$$B_{ij} = w_j - \frac{k_d}{\pi}T_{ij}; \quad \text{if } j < i$$

$$B_{ii} = \frac{1}{2}w_j - \frac{k_d}{\pi}\sum_{k=1}^{N} T_{ik} - \frac{k_d}{2\pi}g(x_{0i})\log\frac{1-x_{0i}}{1+x_{0i}}; \qquad \text{if } i = j$$

$$B_{ij} = -\frac{k_d}{\pi}T_{ij}; \quad \text{if } j > i$$

Solve:
$$\sum_{j=1}^{n} B_{ij}g_j - Ax_{0i} = 0$$

Find: $\forall \hat{x}_k \in \Omega \setminus \Gamma$, with $k = 1, ..., M$

$$B_{ij} = \left[\frac{t_j - \hat{x}_i}{|t_j - \hat{x}_i|^2} - \frac{t_j + \hat{x}_i}{|t_j + \hat{x}_i|^2}\right]$$

then $p(\hat{x}_i) = Ax_i + \frac{k_d}{2\pi k}\sum_{1}^{N} w_j g_j B_{ij}(t_j, \hat{x}_i)\,.$

END

(4.1)

$$\int_V \nabla(\delta\boldsymbol{u}) : \boldsymbol{\sigma}\mathrm{d}V - \int_{\partial_t\Omega} \delta\boldsymbol{u}\cdot\bar{\boldsymbol{t}}\mathrm{d}x^* + \int_\Gamma [\![\delta\boldsymbol{u}]\!] p\boldsymbol{n}^\Gamma \mathrm{d}x^* = 0$$

$$\int_V \delta p\frac{\partial p}{\partial t}\frac{1}{K_f}\mathrm{d}V + \int_V n\delta p\nabla\cdot\boldsymbol{v}_s\mathrm{d}V - \int_V \boldsymbol{w}\cdot\nabla\delta p\mathrm{d}V + \int_\Gamma [\![\delta p\boldsymbol{w}]\!]\cdot\boldsymbol{n}^\Gamma\mathrm{d}x^* + \int_\gamma \delta pq^p\,\mathrm{d}x^* = 0$$

(4.2)

$$\int_\Gamma \delta p\frac{\partial(2h\rho_f)}{\partial t}\mathrm{d}x^* + \int_\Gamma \delta p\rho_f\boldsymbol{v}_s\cdot\boldsymbol{n}_\Gamma\mathrm{d}x^* + \int_\Gamma \delta p\rho_f[\![\boldsymbol{w}]\!]\cdot\boldsymbol{n}_\Gamma\mathrm{d}x^* + \int_\Gamma \delta p\nabla_{x^*}\cdot(\rho_f\boldsymbol{q})\mathrm{d}x^* = 0$$

with $n = 1$ in Γ, $\boldsymbol{w} = n(\boldsymbol{v}_f - \boldsymbol{v}_s)$ the fluid relative velocity, $[\![\delta\boldsymbol{u}]\!] = [\delta\boldsymbol{u}^- - \delta\boldsymbol{u}^+]$ and since we have assumed that the pressure is constant through the thickness of the crack we can write $[\![\delta p\boldsymbol{w}]\!] = \delta p[\![\boldsymbol{w}]\!]$.

Considering the local coordinate system in the center of the crack (see Figure 2), since the crack aperture is much smaller than the crack length, the first integral over Ω^* can be calculated as follows,

$$
\begin{aligned}
\int_{\Omega*} \delta p \nabla \cdot \boldsymbol{v}_s \mathrm{d}\Omega &= \int_\Gamma \int_{-h}^{h} \delta p \nabla \cdot \boldsymbol{v}_s \mathrm{d}y^* \mathrm{d}x^* \\
&= \int_\Gamma \delta p 2h \left\langle \frac{\partial \boldsymbol{v}_s}{\partial x^*} \right\rangle \mathrm{d}a + \int_\Gamma \delta p [\![\boldsymbol{v}_s]\!] \mathrm{d}x^*
\end{aligned} \tag{4.3}
$$

where we have assumed that the tangential component of the matrix velocity $\boldsymbol{v}_s$ has linear variation along y^*, and the symbol $\langle\cdot\rangle$ represents the average value of the function. Also, the tangential derivative of the pressure does not vary along y^* since the pressure is assumed constant through the crack thickness.
Analogously, introducing the Poiseuille law for the fluid (2)

$$
\int_{\Omega^*} k_d \nabla \delta p \cdot \nabla p \, \mathrm{d}v = \int_\Gamma \left(\int_{-h}^{h} k_d \nabla \delta p \cdot \nabla p \, \mathrm{d}y^* \right) \mathrm{d}x^* = \int_\Gamma 2h \, k_d \frac{\partial \delta p}{\partial x^*} \frac{\partial p}{\partial x^*} \mathrm{d}x^* \tag{4.4}
$$

and similarly we deduce

$$
\int_{\Omega^*} \delta p \frac{1}{K_f} \frac{\partial p}{\partial t} \mathrm{d}v = \int_\Gamma \delta p \, 2h \frac{1}{K_f} \frac{\partial p}{\partial t} \mathrm{d}x^* \tag{4.5}
$$

The fluid tht enters into the crack cavity, flows then tangential to it, therefore, the normal flow is discontinuous and also the pressure gradient normal to the crack

$$
\begin{aligned}
\int_\Gamma \delta p [\![\boldsymbol{v}_f - \boldsymbol{v}_s]\!] \cdot \boldsymbol{n}^\Gamma \, \mathrm{d}x^* &= -\int_\Gamma \delta p 2h \left\langle \frac{\partial \boldsymbol{v}_s}{\partial x^*} \right\rangle \mathrm{d}x^* - \int_\Gamma \delta p [\![\boldsymbol{v}_r]\!] \, \mathrm{d}x^* + \\
&\quad + \int_\Gamma 2h \, k_d \frac{\partial \delta p}{\partial x^*} \frac{\partial p}{\partial x^*} \mathrm{d}x^* - \int_\Gamma \delta p \, 2h \frac{1}{K_f} \frac{\partial p}{\partial t} \mathrm{d}x^*
\end{aligned} \tag{4.6}
$$

4.2. **Space and time discretization of the coupled problem.** As to spatial discretization, the domain Ω is dicretized into finite elements, where for each specific element the displacement and pore pressure are interpolated by using shape functions N^I_{ar} y N^I_{pr} (with I the node within the element and $r = 1$ for standard interpolation functions and $r = 2, 3$ for enrichment function associated with discontinuity and near tip sigularity interpolation functions, respectively), of the form

$$
\begin{aligned}
\boldsymbol{u} \approx \boldsymbol{u}^h(\boldsymbol{x}) &= \textstyle\sum_{i\in I} N^i_{a1}(\boldsymbol{x}) \, \boldsymbol{u}^i_1 + \sum_{j\in J} N^j_{a2}(\boldsymbol{x}) \, \boldsymbol{u}^j_2 + \sum_{k\in K} N^k_{a3}(\boldsymbol{x}) \, \boldsymbol{u}^k_3 \\
p \approx p^h(\boldsymbol{x}) &= \textstyle\sum_{i\in I} N^i_{p1}(\boldsymbol{x}) \, p^i_1 + \sum_{j\in J} N^j_{p2}(\boldsymbol{x}) \, p^j_2 + \sum_{k\in K} N^k_{p3}(\boldsymbol{x}) \, p^k_3
\end{aligned} \tag{4.7}
$$

where I denote the set of standard finite element nodes, J enrichment nodes related to the Heaviside step function and K enrichment nodes related to the near tip asymptotic function, $(\boldsymbol{u}^i_1, p^i_1)$ conventional displacement and pressure values of node i, $(\boldsymbol{u}^j_2, p^j_2)$ and $(\boldsymbol{u}^k_3, p^k_3)$ are the additional nodal values of displacement and pressure related to the following shape functions

$$
\begin{aligned}
N^j_{a2}(\boldsymbol{x}) &= N^j_{a1}\left(H(\boldsymbol{x}) - H(\boldsymbol{x}_j)\right) \qquad & N^k_{a3}(\boldsymbol{x}) &= N^k_{a1}\left(F(\boldsymbol{x}) - F(\boldsymbol{x}_k)\right) \\
N^j_{p2}(\boldsymbol{x}) &= N^j_{p1}\left(Z(\boldsymbol{x}) - Z(\boldsymbol{x}_j)\right) \qquad & N^k_{p3}(\boldsymbol{x}) &= N^k_{p1}\left(G(\boldsymbol{x}) - G(\boldsymbol{x}_k)\right)
\end{aligned} \tag{4.8}
$$

where H denote the Heaviside step shape function centered at the discontinuity and Z denote the distance functions, F y G are enhaced basis defined as follows as follows

$$
H = \begin{cases} 1 & \text{if} \quad \boldsymbol{x} \in \Omega^+ ; \\ -1 & \text{if} \quad \boldsymbol{x} \in \Omega^- . \end{cases} \qquad Z = \begin{cases} d & \text{if} \quad \boldsymbol{x} \in \Omega^+ ; \\ -d & \text{if} \quad \boldsymbol{x} \in \Omega^- . \end{cases} \tag{4.9}
$$

$$
\begin{aligned}
\{F(r,\theta)\}_{l=1}^{4} &= \{\sqrt{r}\cos\theta/2, \sqrt{r}\sin\theta/2, \sqrt{r}\sin\theta/2\sin\theta, \sqrt{r}\cos\theta/2\sin\theta\} \\
G(r,\theta) &= \sqrt{r}\sin\theta/2
\end{aligned} \tag{4.10}
$$

with r the distance to the crack tip, θ angle with the crack direction.
In order to accommodate the propagation of discrete cracks through elements, Belytschko used the partition of unity property of the finite element shape function N_i, i.e. $\sum_{i=1}^{n} N_{a\,i} = 1$ with n the number of nodal points in an element. The crack is then seen as a discontinuity in the displacement field, and the displacement can be written as the sum of two continuous displacement fields

$$
\begin{aligned}
\boldsymbol{u} &= \boldsymbol{N}_{a1}\boldsymbol{a}_1 + \boldsymbol{N}_{a2}\boldsymbol{a}_2 + \boldsymbol{N}_{a3}\boldsymbol{a}_3 \qquad p = \boldsymbol{N}_{p1}\boldsymbol{p}_1 + \boldsymbol{N}_{p2}\boldsymbol{p}_2 + \boldsymbol{N}_{p3}\boldsymbol{p}_3 \\
\nabla\boldsymbol{u} &= \boldsymbol{B}_{a1}\boldsymbol{a}_1 + \boldsymbol{B}_{a2}\boldsymbol{a}_2 + \boldsymbol{B}_{a3}\boldsymbol{a}_3 \quad \nabla p = \boldsymbol{B}_{p1}\boldsymbol{p}_1 + \boldsymbol{B}_{p2}\boldsymbol{p}_2 + \boldsymbol{B}_{p3}\boldsymbol{p}_3
\end{aligned} \tag{4.11}
$$

where $\boldsymbol{N}$ and $\boldsymbol{B} = \nabla\boldsymbol{N}$ denotes the standard shape functions and gradient of the shape functions respectively, whereas $\boldsymbol{a}_1$, $i = 1, 2, 3$, contains the conventional and additional degrees of freedom

$$
\begin{aligned}
\boldsymbol{v}_s &= \boldsymbol{N}_{a1}\dot{\boldsymbol{a}}_1 + \boldsymbol{N}_{a2}\dot{\boldsymbol{a}}_2 + \boldsymbol{N}_{a3}\dot{\boldsymbol{a}}_3 \quad \nabla\cdot\boldsymbol{v}_s = \boldsymbol{m}^T(\boldsymbol{B}_{a1}\boldsymbol{a}_1 + \boldsymbol{B}_{a2}\boldsymbol{a}_2 + \boldsymbol{B}_{a3}\boldsymbol{a}_3) \\
\dot{p} &= \boldsymbol{N}_{p1}\dot{\boldsymbol{p}}_1 + \boldsymbol{N}_{p2}\dot{\boldsymbol{p}}_2 + \boldsymbol{N}_{p3}\dot{\boldsymbol{p}}_3 \qquad \nabla\dot{p} = \boldsymbol{B}_{p1}\dot{\boldsymbol{p}}_1 + \boldsymbol{B}_{p2}\dot{\boldsymbol{p}}_2 + \boldsymbol{B}_{p3}\dot{\boldsymbol{p}}_3
\end{aligned} \tag{4.12}
$$

(4.13)

$$
\int_\Omega \boldsymbol{B}_{ai}^T\boldsymbol{\sigma}\,\mathrm{d}V + \int_\Gamma p\boldsymbol{N}_{ai}^T\boldsymbol{n}_\Gamma\,\mathrm{d}x^* - \int_{\partial_t\Omega}\boldsymbol{N}_{ai}^T\bar{\boldsymbol{t}}\,\mathrm{d}x^* = 0
$$

$$
\int_\Omega \boldsymbol{N}_{pi}^T\nabla\cdot\boldsymbol{v}_s\,\mathrm{d}V + \int_\Omega \boldsymbol{N}_{pi}^T\frac{\partial p}{\partial t}\frac{1}{K_f}\,\mathrm{d}V - \int_\Omega \boldsymbol{B}_{pi}^T\boldsymbol{w}\,\mathrm{d}V + \int_\Gamma \boldsymbol{N}_{pi}^T[\![\boldsymbol{w}]\!]\cdot\boldsymbol{n}\,\mathrm{d}x^* + \int_{\partial\Omega}\boldsymbol{N}_{pi}^T\bar{q}\,\mathrm{d}x^* = 0
$$

with $i = 1, 2, 3$. Tractions, pressure and pressure test function have unique values across the discontinuity.
The constitutive laws are then introduced.

$$
\begin{aligned}
\boldsymbol{\sigma} &= \boldsymbol{D} : \boldsymbol{\varepsilon} - \alpha p\mathbf{1} \\
\boldsymbol{w} &= -k\nabla p
\end{aligned} \tag{4.14}
$$

The following coupled set of equations can be obtained as

$$
\boldsymbol{C}\dot{\boldsymbol{x}} + \boldsymbol{K}\boldsymbol{x} + \boldsymbol{f} = \mathbf{0} \tag{4.15}
$$

where $\boldsymbol{x}^T = [\boldsymbol{a}_1, \boldsymbol{a}_2, \boldsymbol{a}_3, p_1, p_2, p_3]$ vector of nodal unknowns. The definition of de matrices $\boldsymbol{C}$, $\boldsymbol{K}$ and $\boldsymbol{f}$ is given in Appendix XX.
The time discretization using the backward Euler integrated format of the mass and linear momentum balance relation has the form

$$
\boldsymbol{F}_{n+1} = \boldsymbol{C}_{n+1}\frac{\Delta\boldsymbol{x}}{\Delta t} + \boldsymbol{K}_{n+1}\boldsymbol{x}_{n+1} + \boldsymbol{f}_{n+1} = \mathbf{0} \tag{4.16}
$$

with $\Delta\boldsymbol{x} = \boldsymbol{x}^{n+1} - \boldsymbol{x}^n$, $\Delta t = t^{n+1} - t^n$, and ($\boldsymbol{x}^{n+1}$,$\boldsymbol{x}^n$) denote the unknowns at time t^{n+1} and t^n, respectively.
The equations as stated in (4.16) are conveniently solved using Newton–Raphson iterations.

5. Numerical examples

Four examples are presented in the following subsections. The first three have a single crack inside the porous matrix with different boundary conditions, i.e. of Neumann and Dirichlet type. The aim is to study the quality of the simulations using XFEM, related to the semianalytical. Both methods were implemented in MATLAB codes.
As fourth example, experimental measurements of flow inside cylinder made of cement paste with a slot of 0.02mm thickness are reported and reproduced with the X-FEM to calibrate the permeability parameter of the model.

5.1. **Pressure inside the crack is known.** In the present example the model problem shown in Figure 5 is considered, made of porous fluid saturated material with a straight single crack inside the element and bulk permeability $k = 1$. The boundary conditions, shown in Figure 5, prescribes $\bar{p} = 0$ along the boundary $\partial_p\Omega$ and $\bar{p} = 1$ inside the crack Γ.
For the X-FEM method, the domain has been discretized using 480 quadrilateral elements. The displacements are interpolated with quadratic shape functions whereas the pressure adopts linear functions. To reproduce the discontinuous displacement field, between 36 and 100 integration points are adopted. The displacement boundary conditions are also introduced to avoid rigid movements.
For the semianalytical approach, 92 integration points have been used for the integration along the discontinuity line. The boundary condition in Γ is $p^{\pm} = 1$ with $p_\infty = 0$.

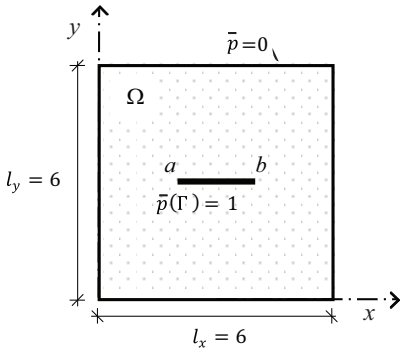

Figure 5. Single crack with prescribed pressure inside the crack.

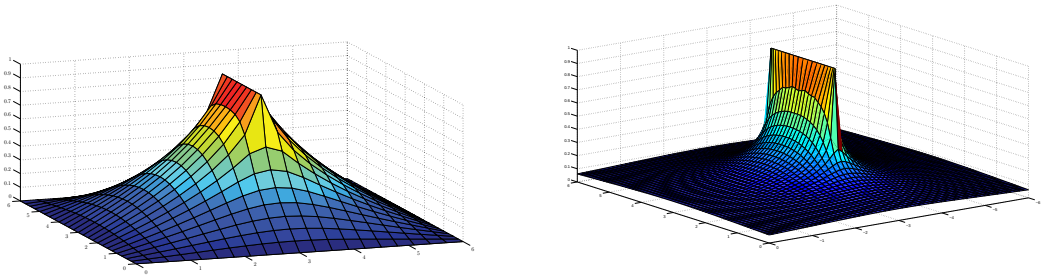

(a) (b)

Figure 6. Pressure field distribution: (a) the X-FEM and (b) the semi-analytical numerical method.

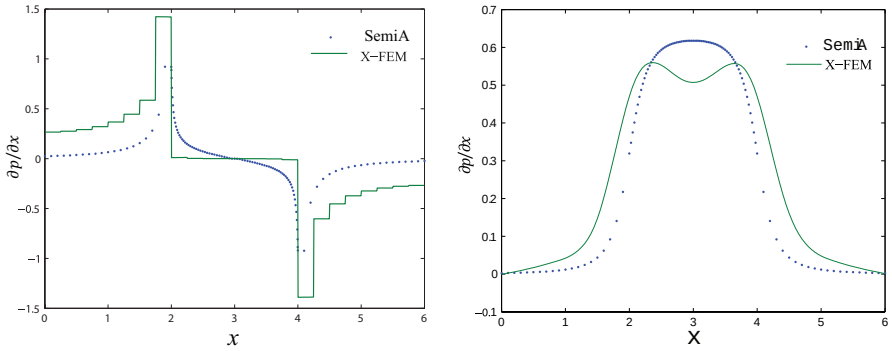

(a) (b)

FIGURE 7. Pressure gradient: (a)$\partial p/\partial x$ along $y = 2.7$;(b)$\partial p/\partial y$ along $y = 3$.

The calculated pressure distribution is depicted in Figure 6 using X-FEM and semi-analitical approach, respectively. We note that a more localize pressure distribution is obtained with the semianalytical approach than with the X-FEM, for the same permeability and zero pressure at infinity and $\partial_p\Omega$, respectively. This is because, the X-FEM has been used on the displacement field, but the constant pressure applied on the crack opposite faces has been considered as Dirichlet boundary condition on the pressure field, no enrichemnt of the pressure field hs been considered. The pressure distribution on the finite element is then linear also over the displacement enriched elements. This is also verified in Figure 7 (a) and (b), where the pressure gradients along lines parallel to the crack direction are shown, i.e. $\partial p/\partial x$ along $y = 2.7$ and $\partial p/\partial y$ along $y = 3$, respectively. XFEM gives higher gradient values far from the discontinuity, in both cases, and a hat shape due to the presence of the crack tips. This result should be improved specially with regards to the perpendicular fluid flow near the crack tip. The pressure gradient $\partial p/\partial y$ verifies, for both approaches, the condition of zero total flow inside the discontinuity.
To analyze the quality of the approximation, the problem has been solved semianalytically using different number of integration points N and with XFEM,increasing the number of elements used in the discretization. In Figure 8 the percentage of absolute relative error is shown for both cases, showing that the solution that gives less than 5% error is between $N = 152$ and $N = 92$, for the seminalytical method and xxx elements for X-FEM.

5.2. **Poiseuille flow inside a crack.** The second model problem considers a permeable solid matrix with $l_x = 6$ and $l_y = 4$ and the same material and flow properties as the previous example, i.e. $E = 30$, $\nu = 0.2$, $b = 1$, $K_f = 1E18\,GPa$ and $k = 1$. In this case, the crack is placed parallel to the axis y as shown in Figure 9.a. Assuming a pressure gradient equal to one, the pressure on the upper boundary at $y = 4$ is $p = 4$ and zero at $y = 0$. On the lateral faces, no fluid is allowed to flow normal to the boundary, i.e. $q = 0$. The problem has symmetry with respect to the axis x, therefore half of the problem will be solved. Analogously to the previous example, the displacement field is restrained to avoid rigid movements. For the seminalytical approach, 60 integration points have been used along the discontinuity line. The boundary conditions are: $\bar{p}(0, y) = 0$ and $p_\infty = Ax$.
Figure 9(b) shows the pressure distribution for $\lambda = 1$. Assuming a high conductivity inside the crack ($k_d = 6.28$ or $\lambda = 1$), an intermediate ($k_d = 0.628$ ro $\lambda = 0.1$) and

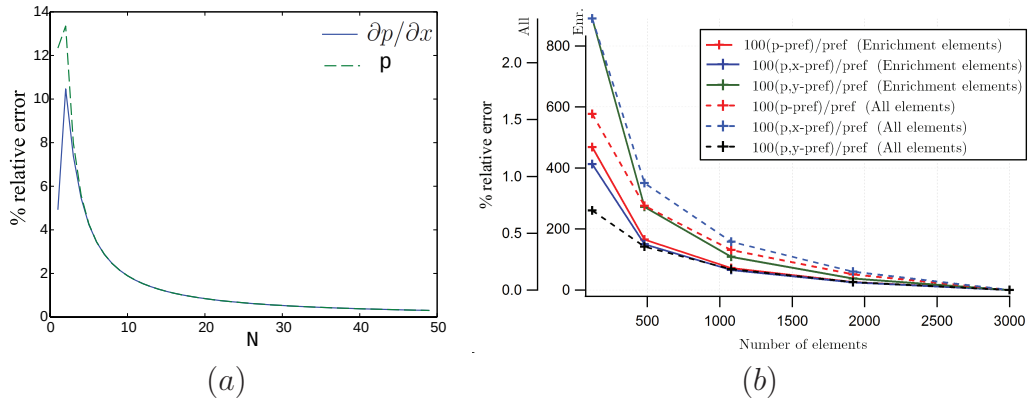

(a) (b)

FIGURE 8. Absolute relative error of the pressure and fluid flow obtained with different number of integration points(a) and with different number of finite elements (b).

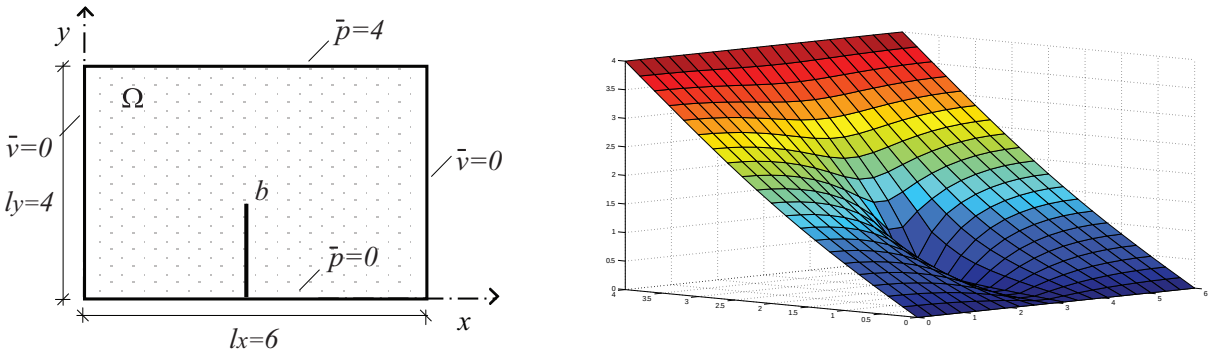

(a) (b)

FIGURE 9. (a)Poiseuille flow inside a crack. (b)Pressure field for a uniform pressure gradient parallel to the crack, with $k = 1$ and $\lambda = 0.01$.

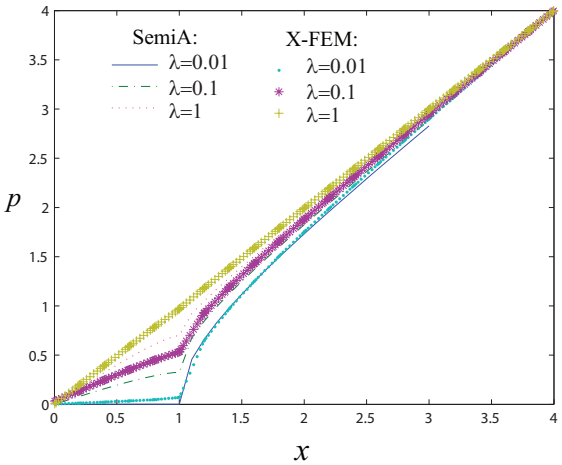

FIGURE 10. Pressure distribution along the crack for different values of λ.

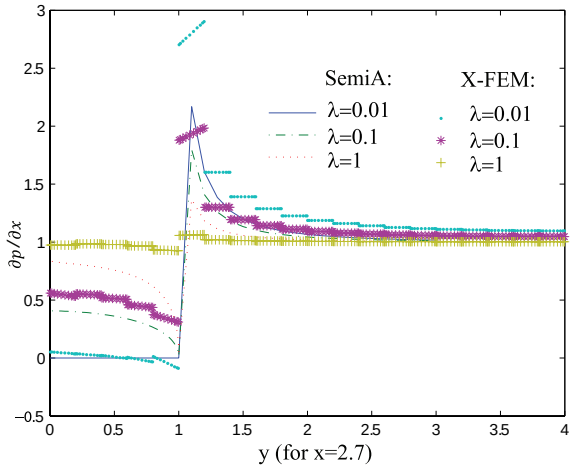

FIGURE 11. Pressure gradient $\partial p/\partial x$ (normal to the crack) along $x = 2.7$ for different values of λ.

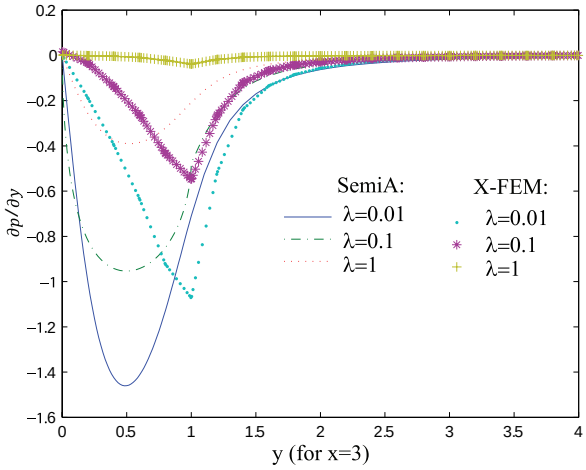

FIGURE 12. Pressure gradient $\partial p/\partial y$ (tangential to the crack) along $x = 3$ for different permeability values.

a low one ($k_d = 0.0628$ or $\lambda = 0.01$). In Figure 10, the pressure distribution along the crack ($x = 3$) is compared. Finally, Figure 11 and Figure 12 show the pressure gradient $\partial p/\partial x$ along $x = 2.7$ and $\partial p/\partial y$ along $x = 3$, respectively.

5.3. **Coupled problem.** In this example the model problem of Figure 13 will be solved assuming that the porous media is elastic, and the mechanical behaviour is coupled to the fluid flow inside the porous matrix. Therefore, the crack opening will be analysed for different permeability coefficients, using XFEM. Let the crack be parallel to the axis y and on the upper face t $y = 6$ a prescribed pore pressure of $p = 6$ is assumed, as shown in Figure 13.a.
Figure 13.b, 13.c and 13.d, show pressure distribution for different permeability values: $k_d = 6.28, 0.628, 0.0628$, i.e. $\lambda = 1, 0.1, 0.01$. Figure 14, show the pressure distribution along a central line that passes along the crack. Figure 15 show the pressure gradient normal to the crack along a parallel line placed at $x = 2.7$. Figure 16 show a pressure gradient tangential to $x = 3$. Coupling the pressure field with the displacement field,

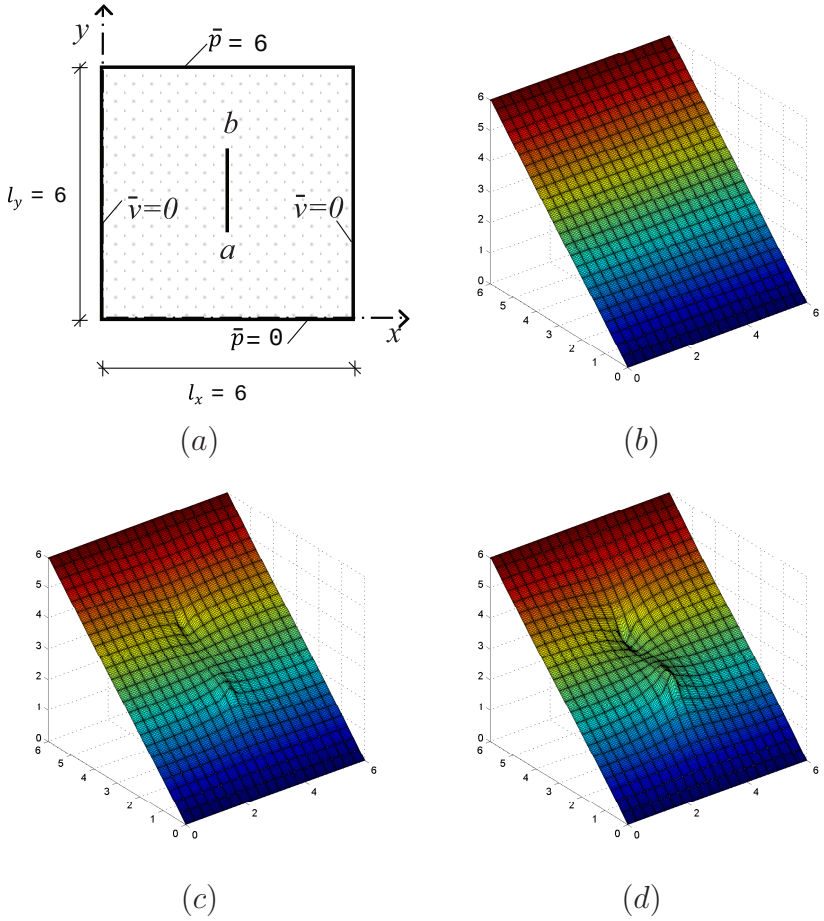

FIGURE 13. (a)Poiseuille flow inside an internal crack. (b),(c) y (d)Pressure field distribution for a uniform pressure gradient prallel to the crack $\lambda = 1$, $\lambda = 0.1$ and $\lambda = 0.01$.

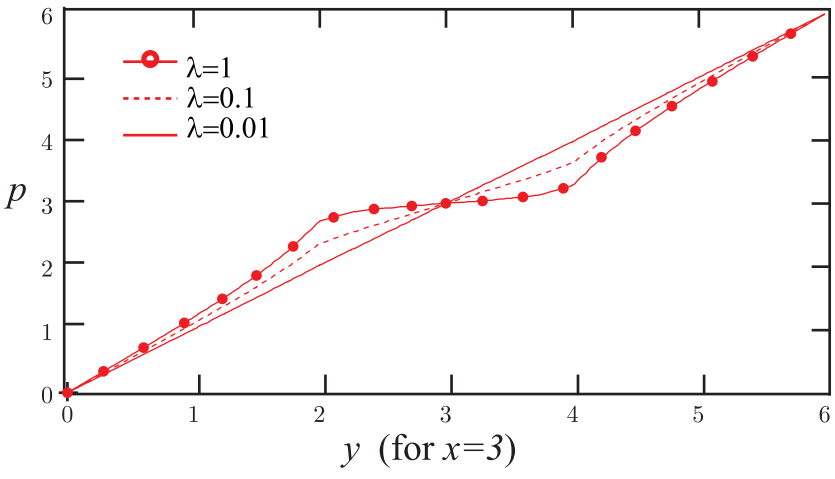

FIGURE 14. Pressure along the crack for different values of λ.

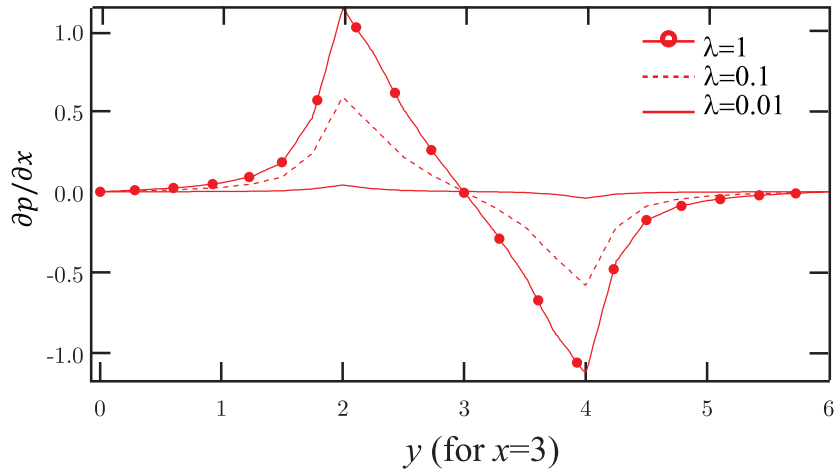

FIGURE 15. Pressure gradient along x direction for different values of λ.

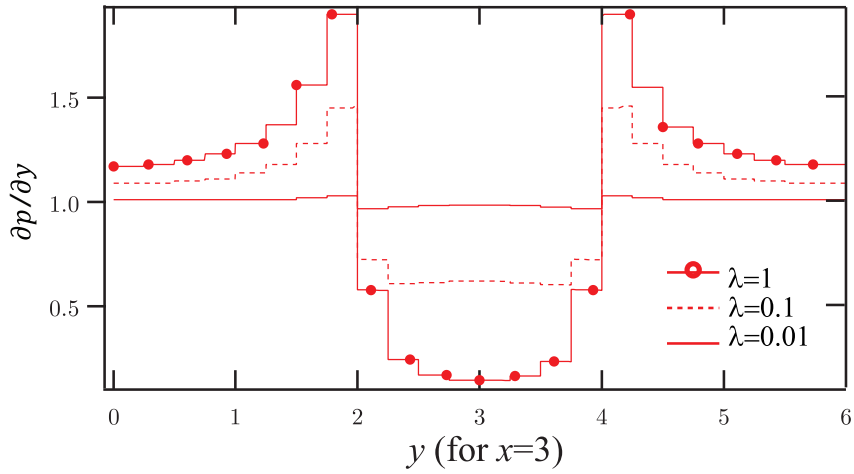

FIGURE 16. Pressure gradient along y direction for different values of λ.

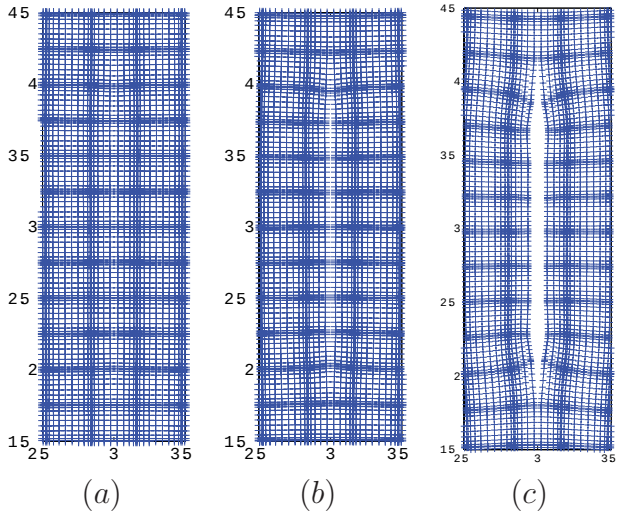

FIGURE 17. Crack aperture due to fluid flow for (a)$\lambda = 1$, (b)$\lambda = 0.1$ y (c)$\lambda = 0.01$.

an additional aperture of the crack is obtained. In Figure **??** the Gauss point position near the crack is shown.

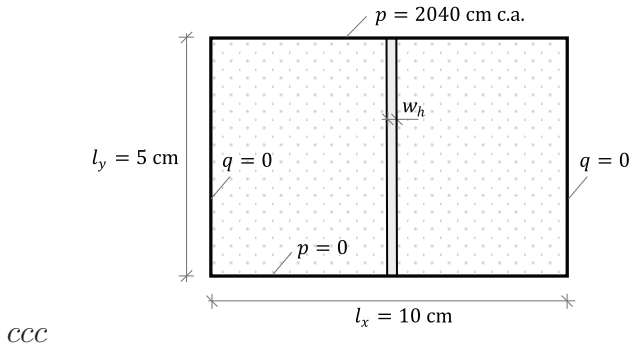

ccc

(*a*) (*b*)

FIGURE 18. Permebility test: (*a*) Geometry and (*b*) model problem.

5.4. **Permeability test.** The transport properties of a porous media that can be used to characterize the internal structure of a porous material are: the water absortion, capillary bsortion, water penetration and coefficient of water permeability. Since the presence of cracks have strong impact on the this properties, in this example cement paste cylinders of approaximately
The aim of this example is to calibrate the coefficient of permeability of a cement paste specimen with a vertical slot placed in the center of it. See Figure 18 and [] for further details on the experimental program that has been carried out following CPC RILEM 13.1. The number of specimens that has been tested is four of $50mm$X$150mm$, and slots of $0.02mm$ thick, $50mm$ height and 10, 20, 30 and 40mm length. To evaluate the permeability, a ring of 25mm thickness, at the upper and lower faces, together with the lateral faces were painted with water proof paint to avoid water loses and ensure vertical flow. Applying and initial water pressure of of 0.1MPa, the pressure is later increased until a stable flow is reached.
To carry out numerical simulations of this experimental test using X-FEM, we consider the model problem shown in Figure 18 with a the central slot. We discretize the domain using 456 mixed finite elements with biquadratic shape interpolation functions for the displacement and bilinear for the pressure. The number of integration points are taken between 36 and 100. Assuming an isotropic uniform permeability of $k_m = 1e-10cm/s$, Biot's coefficient $\alpha = 1$ and compressibility modulus of $Q = 1e18GPa$, ae cuasi incompressible behaviour is considered for the water. The elastic properties for the solid material are $E = 11GPa$ and $\mu = 0,2$, for the Young Modulus and Poisson coefficient, respectivelly. For fluid flow insidede the discontinuity, friccion coefficients of $f = 1.00$ and $f = 1.65$ are considered and dynamic viscocity of the water of $\mu = 1.10^{-7}Ns/cm^2$.
This example assumes Dirichlet boundary conditions, i.e. prescibed pressure at the upper face of $p = 2040cmc.a.$ and $p = 0$ at the lower face. With unidirectional vertical water flow. To avoid rigid body movements, displacements of the lower and later faces are restrained as shown in Figure 19. Numerical results obtained on the permeability coefficient are depicted in Figure 19 showing good agreement with the experimental ones.

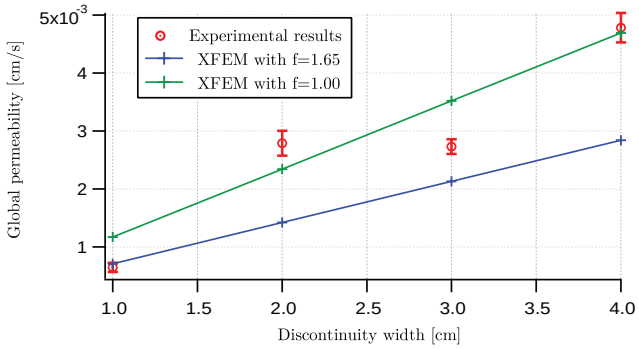

(a) (b)

FIGURE 19. Permeability test: numerical with XFEM and experimental results obtained for different slot length.

6. Concluding remarks

In this paper we have first formulated the problem of fluid flow through fractured deformable porous media. With the aim of solving numerically this problem in a coupled way, we have choosen the XFEM introduced by []. Since the analitical solution of the problem is in terms of a singular integral (Cauchy type integral), a semianalytical approach has been used to solve a simplified problem and compared the results with the one obtained with XFEM. Then four examples have been developed. In the first two, a rigid porous matrix with a single crack is considered assuming Dirichlet and Neumann boundary conditions, respectively. Pressure and gradient pressure results have been compared using both methods, plotting also the absolute relative error for increasing number of discretization points. Results agree quite well, except for the gradient of the pressure near the singularities. Particular interest has been given to the enrichment function used for the pressure, since the calculation of gradient of the pressure appears as delicate issue. The third example aim is to solve the coupled problem but assuming an elastic porous material, showing the hability of the problem to simulate the the increment of pressure and consequent apperture of the crack by incresing the conductivity of the crack. The last example depicts the calibration with experimental results of the permeability coefficient using XFEM.

7. Anexo

$$\boldsymbol{C} = \begin{bmatrix} 0 & 0 & 0 & \widehat{\boldsymbol{C}_{a1p1}} & \widehat{\boldsymbol{C}_{a1p2}} & \widehat{\boldsymbol{C}_{a1p3}} \\ 0 & 0 & 0 & \widehat{\boldsymbol{C}_{a2p1}} & \widehat{\boldsymbol{C}_{a2p2}} & \widehat{\boldsymbol{C}_{a2p3}} \\ 0 & 0 & 0 & \widehat{\boldsymbol{C}_{a3p1}} & \widehat{\boldsymbol{C}_{a3p2}} & \widehat{\boldsymbol{C}_{a3p3}} \\ \boldsymbol{C}_{p1a1} & \boldsymbol{C}_{p1a2} & \boldsymbol{C}_{p1a3} & \boldsymbol{C}_{p1p1} + \widehat{\boldsymbol{C}_{p1p1}} & \boldsymbol{C}_{p1p2} + \widehat{\boldsymbol{C}_{p1p2}} & \boldsymbol{C}_{p1p3} + \widehat{\boldsymbol{C}_{p1p3}} \\ \boldsymbol{C}_{p2a1} & \boldsymbol{C}_{p2a2} & \boldsymbol{C}_{p2a3} & \boldsymbol{C}_{p2p1} + \widehat{\boldsymbol{C}_{p2p1}} & \boldsymbol{C}_{p2p2} + \widehat{\boldsymbol{C}_{p2p2}} & \boldsymbol{C}_{p2p3} + \widehat{\boldsymbol{C}_{p2p3}} \\ \boldsymbol{C}_{p3a1} & \boldsymbol{C}_{p3a2} & \boldsymbol{C}_{p3a3} & \boldsymbol{C}_{p3p1} + \widehat{\boldsymbol{C}_{p3p1}} & \boldsymbol{C}_{p3p2} + \widehat{\boldsymbol{C}_{p3p2}} & \boldsymbol{C}_{p3p3} + \widehat{\boldsymbol{C}_{p3p3}} \end{bmatrix} \tag{7.1}$$

$$
(7.2)\quad \boldsymbol{K} = \begin{bmatrix}
\boldsymbol{K}_{a1a1} & \boldsymbol{K}_{a1a2} & \boldsymbol{K}_{a1a3} & \boldsymbol{K}_{a1p1} & \boldsymbol{K}_{a1p2} & \boldsymbol{K}_{a1p3} \\
\boldsymbol{K}_{a2a1} & \boldsymbol{K}_{a2a2} & \boldsymbol{K}_{a2a3} & \boldsymbol{K}_{a2p1} & \boldsymbol{K}_{a2p2} & \boldsymbol{K}_{a2p3} \\
\boldsymbol{K}_{a3a1} & \boldsymbol{K}_{a3a2} & \boldsymbol{K}_{a3a3} & \boldsymbol{K}_{a3p1} & \boldsymbol{K}_{a3p2} & \boldsymbol{K}_{a3p3} \\
0 & 0 & 0 & \boldsymbol{K}_{p1p1} + \widehat{\boldsymbol{K}_{p1p1}} & \boldsymbol{K}_{p1p2} + \widehat{\boldsymbol{K}_{p1p2}} & \boldsymbol{K}_{p1p3} + \widehat{\boldsymbol{K}_{p1p3}} \\
0 & 0 & 0 & \boldsymbol{K}_{p2p1} + \widehat{\boldsymbol{K}_{p2p1}} & \boldsymbol{K}_{p2p2} + \widehat{\boldsymbol{K}_{p2p2}} & \boldsymbol{K}_{p2p3} + \widehat{\boldsymbol{K}_{p2p3}} \\
0 & 0 & 0 & \boldsymbol{K}_{p3p1} + \widehat{\boldsymbol{K}_{p3p1}} & \boldsymbol{K}_{p3p2} + \widehat{\boldsymbol{K}_{p3p2}} & \boldsymbol{K}_{p3p3} + \widehat{\boldsymbol{K}_{p3p3}}
\end{bmatrix}
$$

$$
(7.3)\qquad \boldsymbol{f} = \begin{bmatrix}
\boldsymbol{f}_{a1} \\ \boldsymbol{f}_{a2} \\ \boldsymbol{f}_{a3} \\ f_{p1} \\ f_{p2} \\ f_{p3}
\end{bmatrix}
$$

donde:

$$
\begin{aligned}
\boldsymbol{C}_{p(i)a(j)} &= -\int_{\Omega} \alpha \boldsymbol{N}_{p(i)}^T \boldsymbol{m}^T \boldsymbol{B}_{a(j)} \,\mathrm{d}V \\
\boldsymbol{C}_{p(i)p(j)} &= \int_{\Omega} K_f^{-1} \boldsymbol{N}_{p(i)}^T \boldsymbol{N}_{p(j)} \,\mathrm{d}V \\
\boldsymbol{K}_{a(i)a(j)} &= \int_{\Omega} \boldsymbol{B}_{a(i)}^T \boldsymbol{D} \boldsymbol{B}_{a(j)} \,\mathrm{d}V \\
\boldsymbol{K}_{a(i)p(j)} &= -\int_{\Omega} \alpha \boldsymbol{B}_{a(i)}^T \boldsymbol{m} \boldsymbol{N}_{p(j)} \,\mathrm{d}V \\
\boldsymbol{K}_{p(i)p(j)} &= -\int_{\Omega} k_f \boldsymbol{B}_{p(i)}^T \boldsymbol{B}_{p(j)} \,\mathrm{d}V \\
(7.4)\qquad \widehat{\boldsymbol{C}_{a(i)p(j)}} &= -\int_{\Gamma} \boldsymbol{N}_{p(i)}^T \, 2h \, \boldsymbol{t}_\Gamma \cdot \left\langle \boldsymbol{B}_{a(j)} \right\rangle \,\mathrm{d}s - \int_{\Gamma} \boldsymbol{N}_{p(i)}^T [\![\boldsymbol{B}_{a(j)}]\!] \cdot \boldsymbol{n}_\Gamma \,\mathrm{d}s \\
\widehat{\boldsymbol{C}_{p(i)p(j)}} &= -\int_{\Gamma} \boldsymbol{N}_{p(i)}^T \, \frac{2h}{K_f} \, \boldsymbol{N}_{p(j)} \,\mathrm{d}s \\
\widehat{\boldsymbol{K}_{p(i)p(j)}} &= -\int_{\Gamma} \left(\boldsymbol{B}_{p(i)}^T \cdot \boldsymbol{t}_\Gamma^T \right) \, 2h \, k_d \left(\boldsymbol{t}_\Gamma \cdot \boldsymbol{N}_{p(j)} \right) \,\mathrm{d}s \\
\boldsymbol{f}_{a(i)} &= \int_{\partial_t \Omega} \boldsymbol{N}_{a(i)}^T \overline{\boldsymbol{t}} \,\mathrm{d}s \\
f_{p(i)} &= \int_{\partial \Omega} \boldsymbol{N}_{p(i)}^T \overline{q} \,\mathrm{d}s
\end{aligned}
$$

con $i, j = 1, 2, 3$; $\boldsymbol{m}^T = [1; 1; 0]$; $\boldsymbol{n}_\Gamma$, $\boldsymbol{t}_\Gamma$ vector normal y tangente a la fisura respectivamente.

Acknowledgements

ML, JL and CT gratefully acknowledges the partial financial support of the Argentinian Research Council, CONICET. ML acknowledge the partial financial support of the Argentinian Agency through the Project Prestamo BID PICT PRH 30 N94.

References

[1] C.-M. Aldea, S.P. Shah and A. Karr. Permeability of cracked concrete. Materials and Structure, 32 (1999) 370–376.

[2] F.Armero and C. Callari. Analysis of strong discontinuities in a saturated poro-plastic solid. International Journal for Numerical Methods in Engineering 46 (1999) 1673-1698.

[3] T. Belytschko and T. Black. Elastic crack growth in finite elements with minimal remeshing, International Journal for Numerical Methods in Engineering 45 (1999) 601-620.

[4] M.A. General theory of three-dimensional consolidation. Journal of Applied Physics 12 (1941) 155-164.

[5] R. de Borst, J. Rethore and M.-A. Abellan. 2009. A numerical approach for arbitrary cracks in a fluid–saturated medium. Arch. Appl Mech 75 (2006) 595-606.

[6] R. de Borst, J. Rethore and M.-A. Abellan. 2009. A precis of two–scale approaches for fracture in porous media. In de Borst, R. and Sadowski, T., editors, *Lecture Notes on Composite Materials: Solid Mechanics and its Applications*, Springer Netherlands. pp. 149–171.

[7] O. Coussy, Mechanics and physics of porous solids. Wiley, 2010.

[8] F.Erdogan, G.D.Gupta and T.S.Cook, Numerical solution of singular integral equations. In: Mechanics of Fracture, Vol. 1 Methods of Analysis and Solutions of Crack Problems (edited by G C Sih), Noordhoff, Leyden, the Netherlands, Chap 7 (1973) 368–425.

[9] P.A. Liolios and G.E. Exadaktylos. A solution of steady-state fluid flow in multiply fractured isotropic porous media. International Journal of Solids and Structures 43 (2006) 3960-3982.

[10] N. Moes, J.Dolbow and T.Belytschko, A finite element method for crack growth without remeshing. International Journal for Numerical Methods in Engineering, 46 (1999) 131–150.

[11] T.Mohammadnejad and A.R.Khoei, Hydro-mechanical modeling of cohsive crack propagation in multiphs porous media using the extended finite element method. International Journal for Numerical and Analitical Methods in Geomechanics 10 (2013) 1247-1279.

[12] N.I. Muskhelishvili, Some basic problems in the mathematicsl theory of elasticity. Noordhoff Ltd, Groiningen- Netherlands, 1953.

[13] A. Pouya nad S. Ghabezloo, Flow around a crack in a porous matrix and related problems. Transport in Porous Media 84 (2010) 511-532.

[14] A. Pouya, Three–dimensional flow in fractured porous media: A potential solution based on singular integral equations. Advances in Water Resources 35 (2012) 30-40.

[15] J.R. Rice, M.P. Cleary, Some basic stress diffusion solutions for fluid-saturated elastic porous media with compressible constituents, Reviews of Geophysics and Space Physics, 14 (1976) 227–241.

[16] M.C.Torrijos, G.Giaccio and R.Zerbino, Internal cracking and transport properties in damaged concretes, Materials nd Structures, 43 (2010) 109–121.

†CONICET, INSTITUTO DE ESTRUCTURAS, UNIVERSIDAD NACIONAL DE TUCUMÁN, SAN MIGUEL DE TUCUMÁN, TUCUMÁN, ARGENTINA

⋆CONICET, LEMIT, LA PLATA, BUENOS AIRES, ARGENTINA